

Bombyx mori nucleopolyhedrovirus F-like protein Bm14 is a factor for viral-induced cytopathic effects via regulating oxidative phosphorylation and cellular ROS levels

Xiangshuo Kong, Weifan Xu, Nan Chen, Yang Li, Yunwang Shen, Xiaofeng Wu *

Institute of Sericulture and Apiculture, College of Animal Science, Zhejiang University, Hangzhou, China

ARTICLE INFO

Keywords:

Cytopathic effects
BmNPV
Bm14
Cell detachment
Oxidative stress

ABSTRACT

Bombyx mori nucleopolyhedrovirus (BmNPV) is highly pathogenic to *Bombyx mori*, silkworm, which causes serious cytopathic effects (CPEs) during infection. However, the role of viral protein in the virus-induced CPEs remains unclear. Here, we discovered that BmNPV infection induced severe CPEs including titer-dependent cell floating and changes in cellular surface morphology. Further explorations revealed the involvement of F-like protein (Bm14), a viral envelope protein, in inducing cytotoxicity and detachment of adherent BmN cells, and its disruption significantly impaired the virus infection-mediated CPEs. Intriguingly, transcriptomic analysis identified the tight association of *Bm14* deletion with the activation of cellular oxidative phosphorylation pathway, consistent with the elevated mitochondrial membrane potential (MMP) levels and ATP concentrations as well as reduced ROS levels. Collectively, our results characterized for the first time the novel role of Bm14 in accelerating viral-induced cytopathogenicity via suppressing the cellular oxidative phosphorylation levels and upregulating the ROS levels.

1. Introduction

Baculoviruses represent a large group of insect-specific enveloped viruses, in which the double-stranded DNA genome is assembled into rod-shaped nucleocapsids (Rohrmann, 2019). Baculoviruses have a unique biphasic life cycle which produces two phenotypes of virions, namely the occlusion-derived virus (ODV) and the budded virus (BV) (van Oers and Vlak, 2007). During the whole infection cycle, ODVs establish primary infection in the host midgut and mediate horizontal host transmission, whereas BVs are in charge of the infection of systemic cell propagation within the individual larvae. As a representative member of the *Alphabaculovirus* genus in the *Baculoviridae* family, Bombyx mori nucleopolyhedrovirus (BmNPV) is highly pathogenic and lethal to silkworm, leading to serious damage in the sericulture industry annually (Dong et al., 2015). In Group I NPVs, BVs appear to have a number of envelope proteins including GP64, F-like protein (the homolog of F protein), v-Ubi (Ac35), GP37 (Ac64), ODV-E25 (Ac94), ODV-E18 (Ac143) and BV/ODV-E26 (Ac16) (Blissard and Theilmann, 2018). Of them, GP64 is the major envelope protein responsible for mediating membrane fusion and receptor binding (Dong et al., 2010; Hefferon et al., 1999; Zhou and Blissard, 2008). By contrast, the F-like

proteins, such as Bm14 and Ac23, although related to the fusion proteins of baculovirus lineage that do not encode gp64, lack the conserved domain that harbors the furin-like cleavage sites, with no membrane fusion activity (Pearson et al., 2001; Rohrmann and Karplus, 2001). Previous studies show that Bm14 is a type I integral membrane protein, which functions to regulate the virulence in infected larvae and facilitate the attachment of ODVs to the midgut epithelial cells (Xu et al., 2019; Xu et al., 2020a). In addition, Ac23 appears to influence viral pathogenicity by accelerating the mortality of infected insects (Lung et al., 2003).

Cytopathic effects (CPEs) represent the widespread property and capacity of viruses (Agol, 2012). Specifically, the virus infection-induced CPEs covers different aspects, like membrane system remodeling, cell detachment, cell morphological changes, cell shrinkage, chromatin condensation and syncytia formation (Netherton et al., 2007; Pereira, 1961). These various effects may represent the phenotypes or inducements of virus-modulated innate immune responses. Notably, the apoptosis mediated by baculovirus infection is the most extensively studied innate immune response (Cerio et al., 2010; Schultz and Friesen, 2009). In baculovirus-infected host cells, virus triggers a proapoptotic DNA damage response essential for efficient virus propagation (Huang et al., 2011; Mitchell and Friesen, 2012). Moreover, the hallmarks of apoptosis, such as chromatin condensation

* Corresponding author.

E-mail address: wuxiaofeng@zju.edu.cn (X. Wu).

Abbreviations

BmNPV	Bombyx mori nucleopolyhedrovirus
CPEs	Cytopathic effects
MMP	mitochondrial membrane potential
ATP	Adenosine triphosphate
ROS	reactive oxygen species
ODV	occlusion-derived virus
BV	budded virus
SEM	scanning electron microscopy
DEGs	differentially expressed genes
NAD ⁺	nicotinamide adenine dinucleotide
DCFH-DA	dichlorofluorescin diacetate

and apoptotic body formation, have been detected in baculovirus-infected host hemocytes and fat body (Zhang et al., 2002). Nonetheless, it remains unknown whether other CPEs are induced by BmNPV infection, even though the above CPEs have been widely investigated.

In this study, we verified that BmNPV infection suppressed cell adhesion and triggered host cell floating. Virus envelope proteins have been suggested to be instrumental in causing cell detachment (Francica et al., 2009; Simon and Linstedt, 2018; Yang et al., 2000). Therefore, GP64 and F-like protein (Bm14), the two major envelope proteins of BmNPV, were selected to determine their roles in inducing cell deadhesion. To our surprise, the transient transfection of Bm14, rather than GP64, was able to induce cell detachment and cytotoxicity. Moreover, the *Bm14*-null mutant had declined capacity to induce cell floating and cytotoxicity. RNA-seq results suggested that the oxidative phosphorylation pathway was activated in *Bm14*-null mutant infected cells. Therefore, our results suggest that Bm14 participates in the suppression of the oxidative phosphorylation pathway by influencing reduced MMP levels and ATP concentrations. This reduction in oxidative phosphorylation may accelerate cytopathogenicity by activating ROS levels.

2. Results

2.1. BmNPV infection induced CPEs including cell floating and morphological changes

As a highly pathogenic DNA virus, baculovirus infection induces

several common CPEs, including chromatin condensation, migration and syncytium formation (Katou et al., 2010; Nagamine et al., 2008; Zhang et al., 2002). To explore whether BmNPV infection induce other CPEs, cell detachment assay was conducted. The results showed that the proportion of floating cells gradually increased during BmNPV infection and this increment was mediated in a virus titer-dependent manner (Fig. 1A). Moreover, scanning electron microscopy (SEM) revealed that the normal adherent BmN cells possessed numerous filaments at the plasma membrane surface, whereas the host cells infected with BmNPV at 48 h p.i. resulted in the drastic formation of blebs and disappearance of extracellular filaments at the cell surface (Fig. 1B). Taken together, these results demonstrated that BmNPV infection induced serious virus titer-dependent cell detachment and fundamentally changed the cellular morphology.

2.2. Transient transfection with Bm14 induced cell detachment and cytotoxicity

The high pathogenicity and mortality of baculovirus infection have been noted in a number of studies, but the role of viral factors leading to the detachment of adherent cells remains unknown. As reported by previous studies, viral envelope proteins are crucial in cell de-adhesion mediated by virus infection (Francica et al., 2009; Simon and Linstedt, 2018; Yang et al., 2000). BmNPV possesses two major BV envelope proteins, namely, GP64 and F-like protein. Thus, the functions of these two proteins in triggering cytotoxicity and cell detachment were characterized. In brief, BmN cells were transfected with EGFP, EGFP-GP64, mCherry, and mCherry-Bm14 constructs for 48 h p.t., and the proportion of detached cells was determined (Fig. 2A). These expression plasmids were constructed using pIZ/V5-His plasmid, which contained the *OPIE2* promoter. *egfp* and *mCherry* were independently expressed or fused with *gp64* and *Bm14* using the *OPIE2* promoter, respectively. As controls, the EGFP and mCherry constructs did not exhibit a potential role in inducing cell detachment. Importantly, mCherry-Bm14 transfected cells achieved a significantly higher degree of detachment (~23%) than those of EGFP, EGFP-GP64 and mCherry transfected cells (~10%, ~11% and ~11%, respectively), indicating that Bm14 contributed to inducing cell floating. Moreover, this induction was mediated in a transfection dose-dependent manner (Fig. 2B). Next, we intended to explore whether Bm14 induced cell detachment was associated with cell viability. According to the results, mCherry-Bm14 also showed slight cytotoxic activity, whereas the cell viability was unaffected when mCherry was expressed independently (Fig. 2C). Collectively, these findings suggested that Bm14 was able to induce cell

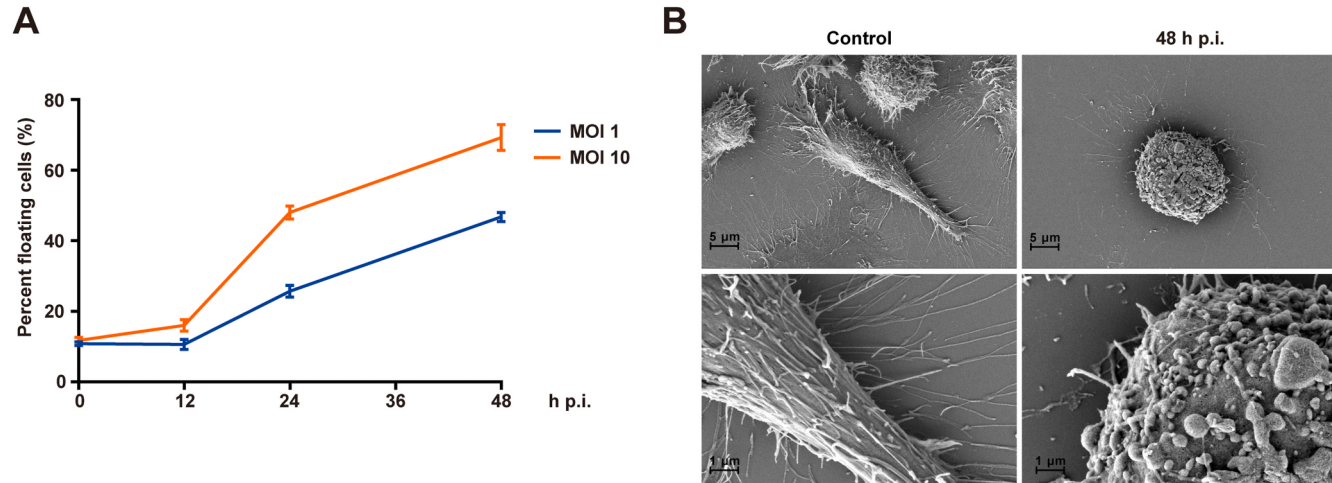


Fig. 1. BmNPV infection induces serious cytopathic effects. (A) BmNPV infection induces severe cell detachment in a viral titer-dependent manner. Each assay was repeated in three individual replicates. (B) SEM of normal BmN cells and BmNPV infected cells. Scale bars indicate 5 μ m (top) and 1 μ m (bottom).

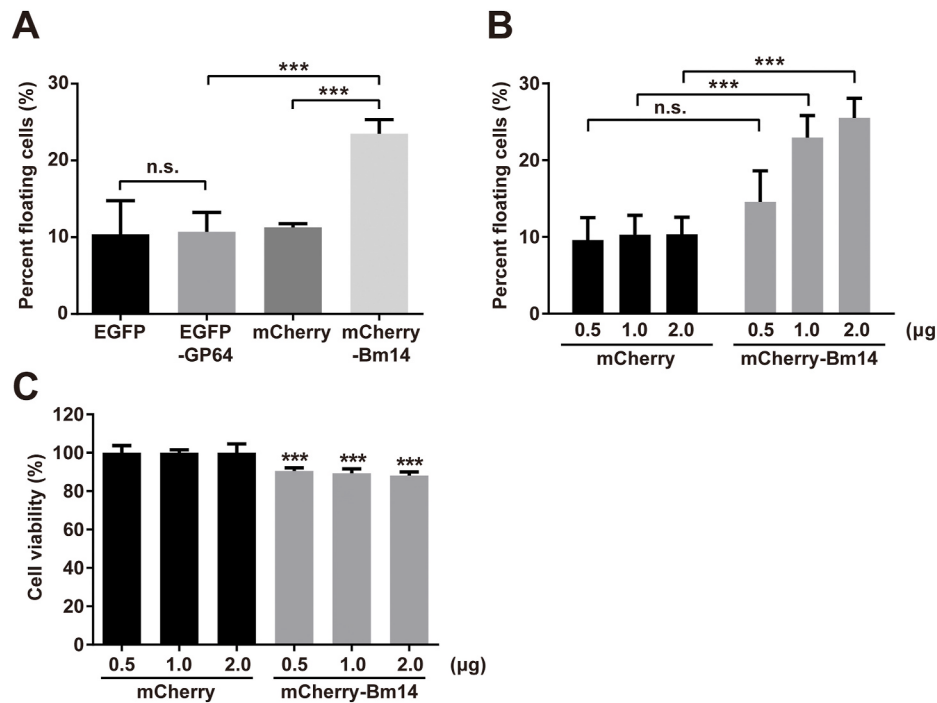


Fig. 2. Transient expression of Bm14 results in cell detachment and cytotoxicity. (A) Detachment of BmN cells transiently transfected with either EGFP, EGFP-GP64, mCherry or mCherry-Bm14 at 48 h p.t. ($\sim 2 \times 10^5$ cells were transfected with 1 μ g plasmid; $n = 3$; ***, $p < 0.001$; n.s., no significant). (B) Bm14 induces detachment in a transfection titer-dependent manner ($\sim 2 \times 10^5$ cells were transfected with mCherry or mCherry-Bm14 construct; $n = 3$; ***, $p < 0.001$; n.s., no significant). (C) Transient transfection of mCherry-Bm14 (% cell viability: 0.5 μ g, ~91%; 1.0 μ g, ~89%; 2.0 μ g, ~88%) triggers slight cytotoxicity relative to mCherry alone(% cell viability: 0.5 μ g, ~100%; 1.0 μ g, ~100%; 2.0 μ g, ~100%; ***, $p < 0.001$). Each assay was repeated in six individual replicates.

detachment and cytotoxicity.

2.3. Bm14 affected cell morphology

To further analyze the ability of Bm14 in causing CPEs, immunofluorescence was performed to determine the precise distribution of the ectopically expressed Bm14 fused with mCherry at 48 h p.t. As observed, the mCherry signals were diffused in the cytoplasm, whereas the signals of anti-Bm14 antibody were concentrated in the filaments on cell surface in addition to being localized with the mCherry (Fig. 3A). We surmised that the difference in distribution of mCherry and Bm14 might be due to the uncharacterized degradation or posttranslational modification of Bm14, which was found in the pellet of OB (Xu et al., 2020a). Such distribution pattern indicated that Bm14 might affect cell morphology via altering the structure of filaments. Moreover, SEM results showed that mCherry-Bm14 transfection at 48 h p.t. led to the formation of short filament-like structures on the cellular surface, whereas mCherry transfection did not affect the cell morphology, suggesting Bm14 might cause the shrinkage or reduction of filaments (Fig. 3B). These results revealed a potential mechanism that Bm14 changed cell morphology through reduction in the size of the extracellular filaments.

2.4. Bm14 deletion reduced the virus infection-triggered CPEs

Subsequently, to determine whether Bm14 exerted a certain role in causing CPEs during BmNPV infection, BmN cells were infected with the recombinant viruses *BmWT*^{PH-EGFP}, *Bm14KO*^{PH-EGFP} or *Bm14Rep*^{PH-EGFP} (Xu et al., 2019) at an MOI of 1 or 10. The *Bm14* knockout virus was constructed via RecE/RecT (ET) homologous recombination and the repaired virus was constructed via Tn7-mediated transposition. Moreover, PH and EGFP were individually expressed and using the *polyhedrin* promoter and *ie1* promoter, respectively. At 24 and 48 h p.i., *Bm14* knockout, relative to the wild type or repair virus, reduced the impact on virus infection-induced cell detachment (Fig. 4A, B). However, it was noticeable that *Bm14*-null mutant still triggered the detachment of adherent cells, suggesting that *Bm14* was not the only factor involved in this process. Meanwhile, cell viability was tested using the MTT assay. The results showed that *Bm14*-null virus also showed relatively lower

cytotoxic activity at MOI 10 than control viruses at 24 and 48 h p.i. (Fig. 4C, D). In addition, to determine whether the absence of *Bm14* affected cell morphology, the cell surface structure was observed by SEM assays. At 48 h p.i., a mass of blebs was found on the plasma membrane of control virus-infected cells, accompanied with the disappearance of extracellular filaments (Fig. 5). However, a distinguishable morphology was observed on the surface of *Bm14*-null mutant infected cells at 48 h p.i. Specifically, on the surface of these cells, we could concurrently observe the presence of thick and straight filaments and the appearance of blebs (Fig. 5). This finding confirmed the result of transient transfection assay that the presence of Bm14 changed the cellular surface morphology (Fig. 3B). Taken together, these results indicated that Bm14 as a viral factor participated in BmNPV-induced cell detachment, cytotoxicity and alterations in cell morphology during infection.

2.5. Genes affected by *Bm14* deletion

To further explore the underlying mechanism by which *Bm14*-null resulted in differences in virus infection caused CPEs, comparative transcriptomic analysis was conducted between *BmWT*^{PH-EGFP} and *Bm14KO*^{PH-EGFP} infected cells at 48 h p.i. In total, 471 differentially expressed genes (DEGs) were identified, among which 42 genes were down-regulated and 429 genes were up-regulated in the *Bm14*-null mutant infected cells (Fig. 6A). Next, the Kyoto Encyclopedia of Genes and Genomes (KEGG, a database resource for understanding high-level functions and utilities of the biological system) pathway enrichment analysis was performed to investigate the biological functions of DEGs. The results showed that the DEGs were significantly enriched in three KEGG pathways (Fig. 6B), including oxidative phosphorylation (bmor00190), phagosome (bmor04145) and glycolysis/gluconeogenesis (bmor00010). qRT-PCR results confirmed that the genes (12/14) enriched in the oxidative phosphorylation pathway were significantly up-regulated in the *Bm14*-null mutant infected cells (Fig. 6C). Specifically, five genes (BGIBMGA004009, BGIBMGA014059, BGIBMGA012356, BGIBMGA002455 and BGIBMGA009182) were subunits of Complex I, which was responsible for the transfer of electrons from NADH to the respiratory chain; two genes (BGIBMGA011593 and BGIBMGA010790) were subunits of Complex II, which was responsible

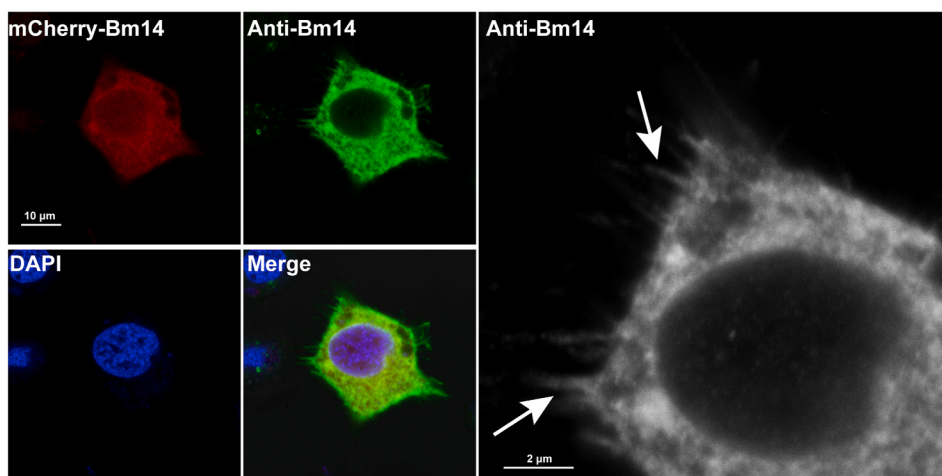
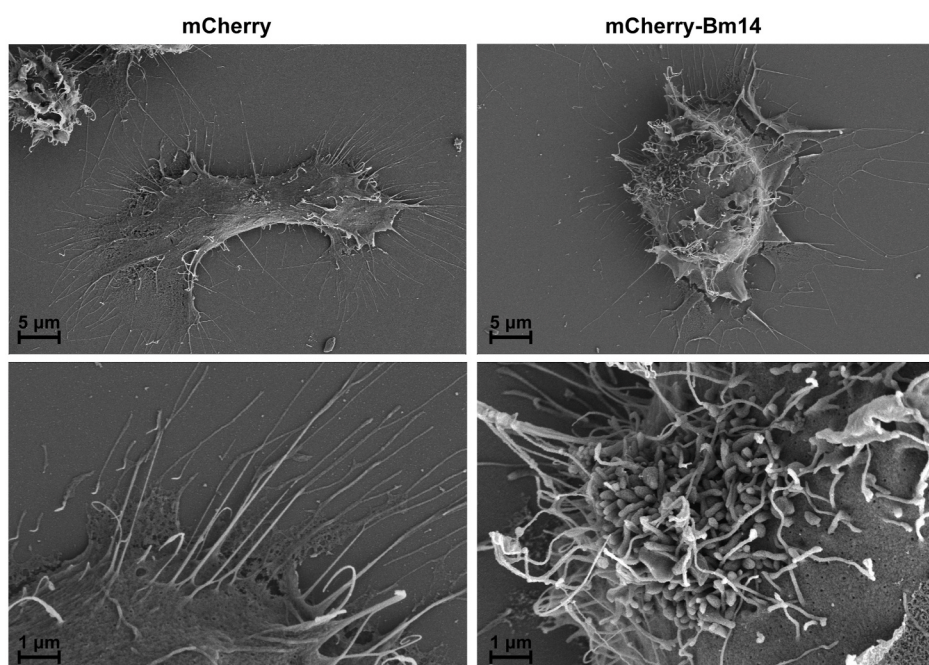
A

Fig. 3. Transfection of Bm14 impacts the morphology of cellular surface. (A) Immunofluorescence analysis of the distribution of transiently transfected with mCherry-Bm14. Red, Bm14 conjugated mCherry; green, anti-Bm14; blue, nucleus; white arrows indicate the filaments on cell surface. (B) SEM analysis of the differences in cellular surface morphology affected by transient transfection of mCherry-Bm14. The filaments were indicated with white arrows. Scale bars indicate 5 μm (top) and 1 μm (bottom).

B

for transferring electrons from succinate to ubiquinone (coenzyme Q); four genes (BGIBMGA013451, BGIBMGA013680, BGIBMGA014175 and BGIBMGA009700) were components of Complex IV, which was involved in oxidative phosphorylation; two ATP synthase genes (BGIBMGA001853 and BGIBMGA012549) were responsible for producing ATP from ADP in the presence of a proton gradient across the membrane; the last gene (BGIBMGA000596) was a subunit of ATPase. This pathway has been demonstrated to play essential roles in energy metabolism and oxidative stress (Table 1). In addition, it produces reactive oxygen species (ROS), which can cause cytotoxicity and impairment to cells (Cole, 2016). Moreover, the glycolysis/gluconeogenesis pathway is another important pathway responsible for energy supply (Melkonian et al., 2020). Taken together, these enrichments and up-regulations indicated that Bm14 might function as a cytopathic effector via altering cellular energy metabolism and regulating the ROS levels.

2.6. Bm14 deletion increased the mitochondrial membrane potential (MMP) levels and ATP concentration

Oxidative phosphorylation occurs in the mitochondrion inner membrane and produces an electrical chemical gradient between the inner and outer mitochondrion membrane. ATP is generated by four complexes of respiratory chain through hydrogen and electron transfer reactions in the mitochondria. Thus, to further determine the function of Bm14 in regulating the oxidative phosphorylation pathway, JC-1 dyeing and ATP assays were conducted to monitor the mitochondrial function during infection with these recombinant viruses. The JC-1 probe exhibits MMP-dependent accumulation in the mitochondria matrix, forming JC-1 aggregates with red fluorescence, however, when the mitochondrial inner membrane becomes depolarized, JC-1 monomers show high green fluorescence (Cossarizza et al., 1993). As shown in Fig. 7A, mock control displayed high red fluorescence (JC-1 aggregates) and low green fluorescence (JC-1 monomers), indicating control cells possessed high MMP values (Fig. 7B) and normal mitochondrial function. CCCP treatment was used as a positive control for indicating low

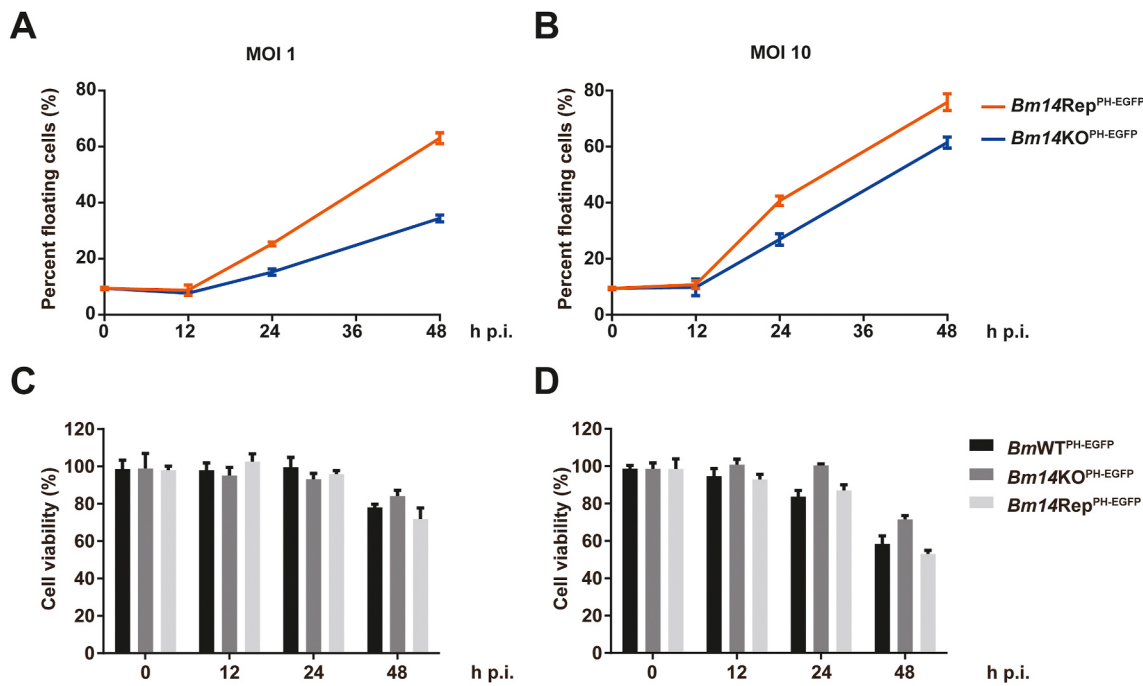


Fig. 4. Bm14 deletion virus reduces virus induced CPEs. (A, B) Detachment assays of BmN cells infected with *BmWT*^{PH-EGFP} and *Bm14KO*^{PH-EGFP} within 48 h p.i. at MOI of 1 or 10, respectively (n = 3). (C, D) MTT assays of BmN cells infected with *BmWT*^{PH-EGFP}, *Bm14KO*^{PH-EGFP} or *Bm14Rep*^{PH-EGFP} at MOI of 1 or 10, respectively (n = 6).

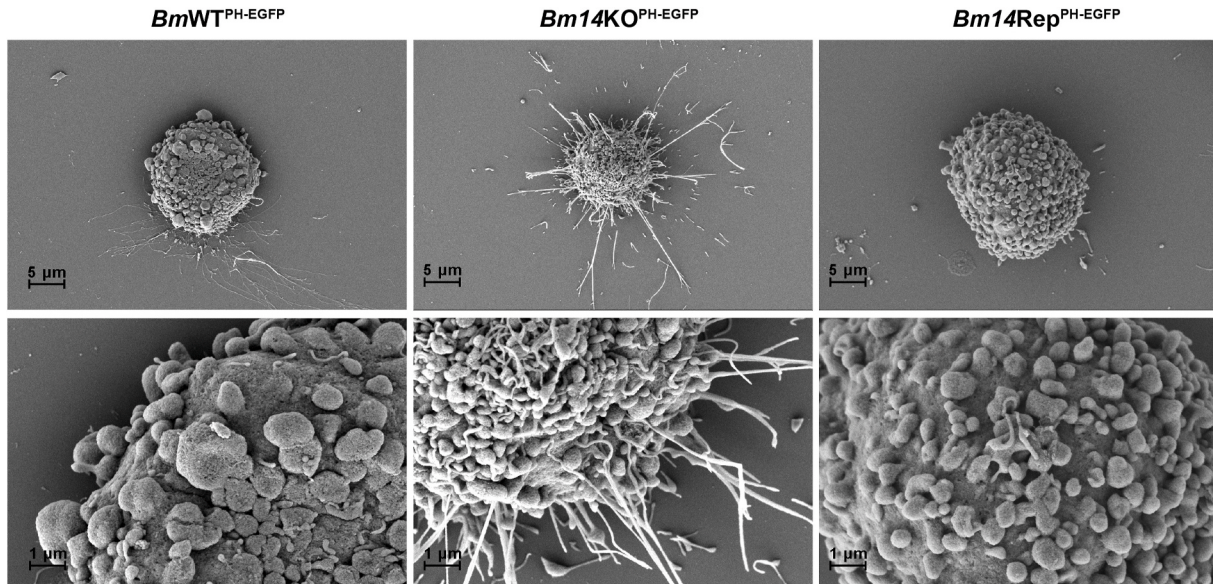


Fig. 5. Bm14 deletion virus affects cellular surface morphology. SEM analysis of BmN cells infected with *BmWT*^{PH-EGFP} (left), *Bm14KO*^{PH-EGFP} (middle) or *Bm14Rep*^{PH-EGFP} (right) at 48 h p.i. Scale bars indicate 5 μm (top) and 1 μm (bottom).

MMP levels and mitochondria dysfunction (Fig. 7A, B). The red signals were attenuated upon *BmWT*^{PH} and *Bm14Rep*^{PH} infection at 48 h p.i., suggesting that virus infection decreased the MMP values and disturbed the mitochondrial function (Fig. 7A, B). In the *Bm14KO*^{PH} mutant-infected cells, however, the red signals were increased and the MMP values recovered to the normal levels at 48 h p.i. (Fig. 7A, B). Moreover, at 48 h p.i., ATP concentrations in *Bm14KO*^{PH} infected cells were significantly higher than in *BmWT*^{PH} and *Bm14Rep*^{PH} infected cells (Fig. 7C). The ATP assay results showed that Bm14 knockout increased ATP concentrations, indicating that Bm14 inhibited the host energy metabolism activity. Collectively, these results revealed the vital roles of

Bm14 in suppressing mitochondria function through regulating MMP levels and ATP concentrations.

2.7. Effects of Bm14 mutant on intracellular ROS levels

Cell death caused by viral infection is a complex process that involves multiple factors and remains poorly understood. In a previous study (Santos et al., 2010), Bm14 was considered to participate in the stress response under viral infection. To examine whether the effect of Bm14 on accelerating larvae and cell death might have more to do with oxidative stress, we measured the intracellular ROS levels induced by

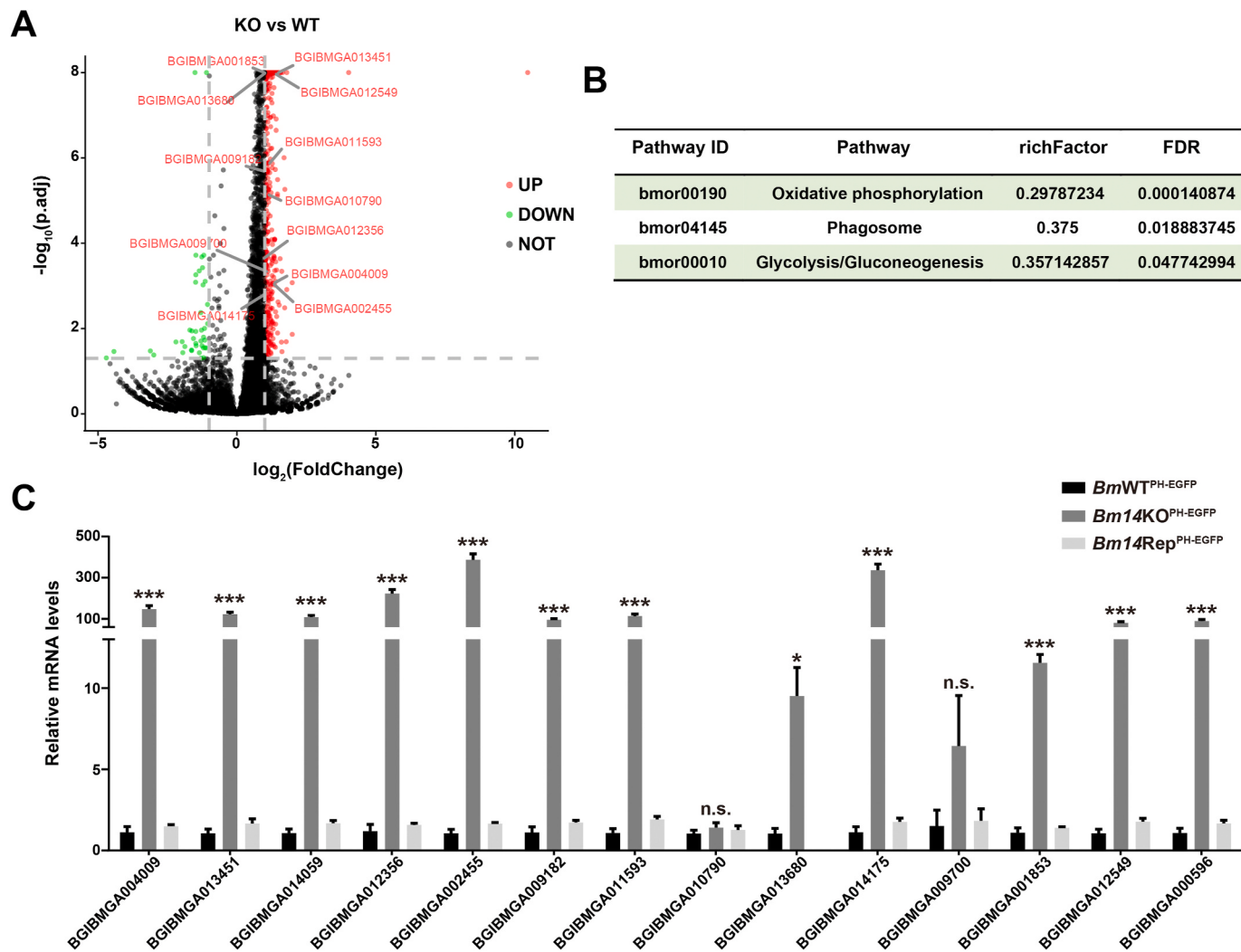


Fig. 6. Transcriptome analysis of DEGs between *BmWT*^{PH-EGFP} and *Bm14KO*^{PH-EGFP} infected cells. (A) Volcano plot of DEGs between KO vs WT. Red plots represent up-regulated genes in KO samples, green plots represent down-regulated genes, black plots represent no significant changed genes. The significant standard is $p.\text{adjust} < 0.05$, $|\text{FoldChange}| \geq 2$. (B) The top three enriched KEGG pathways. The richFactor is the ratio of genes enrichment. FDR, false discovery rate, was calculated using the Benjamini-Hochberg procedure. (C) qPCR analysis of 14 genes enriched in oxidative phosphorylation pathway ($n = 3$; *, $p < 0.05$; **, $p < 0.01$; ***, $p < 0.001$; n.s., no significant).

BmWT^{PH}, *Bm14KO*^{PH} or *Bm14Rep*^{PH} infection using an oxidation-sensitive fluorescent probe (DCFH-DA). As shown in Fig. 8 the intracellular ROS of three recombinant virus-infected cells both maintained a relatively low level from 6 to 24 h p.i. It was not until 48 h p.i. that ROS levels increased obviously. However, although it exhibited the similar tendency in all cases, the levels of cells infected with *Bm14KO*^{PH} were significantly lower in comparisons with those of *BmWT*^{PH} and *Bm14Rep*^{PH} at 48 and 72 h p.i.

3. Discussion

BmNPV and other Group I NPVs have emerged as insect-specific viruses with high pathogenicity, which pose serious lethality to their hosts (Rohrmann, 2019; Zhang et al., 2002). However, the cytopathogenicity induced by these viruses remains unclear so far. In this study, the BmNPV infection-mediated CPEs including cell detachment, changes in cell morphology and cytotoxicity were characterized. We found that Bm14 was one of the viral factors involved in inducing CPEs during ectopic expression and BmNPV infection.

Baculovirus infection induces several typical CPEs, including cell rounding, nuclear hypertrophy and cell detachment (Huang et al., 2019; Kamita and Maeda, 1993; Levin and Huang, 1999; Whittome-Waygood

et al., 2009). Cell detachment, changes in cell morphology and cytotoxicity are typical CPEs induced by virus. It is well known that viral envelope proteins are responsible for the formation of syncytium (Blissard and Wenz, 1992; Mi et al., 2000; Stamatatos and Cheng-Mayer, 1993; Wang et al., 2005), cell detachment (Simon and Linstedt, 2018; Yang et al., 2000) and cytotoxicity (Curtin et al., 2018; McGettigan et al., 2001) during infection processes. Thus, we surmised that the BV major envelope proteins of BmNPV might exert the functions in causing these CPEs. Surprisingly, Bm14 was found to have a direct effect on BmNPV infection-mediated CPEs, instead of GP64. This was interpreted to suggest that Bm14 not only has auxiliary functions in syncytium formation (Xu et al., 2020b), but also plays important roles in other CPEs. To our surprise, Bm14 distributed in the filament on the cellular surface and we proposed an assumption that Bm14 was able to shrink these filaments through unknown mechanisms. In addition, the F protein in group II NPVs show sequence similarity to Bm14 but possesses a conserved furin-like cleavage site and is capable of pH-mediated membrane fusion activity (Lung et al., 2002; Westenberg et al., 2002). These structure and activity features are analogous to Ebola virus glycoprotein, which is shown to be associated with the detachment of infected cells and induction of cytotoxicity (Hacke et al., 2015a). Therefore, we speculated that F proteins possess similar functions as the F-like protein

Table 1

Functions of DEGs enriched in oxidative phosphorylation pathway.

Gene ID	Gene name	Function	Complex of oxidative respiratory chain
BGIBMGA004009	<i>NADH dehydrogenase [ubiquinone] iron-sulfur protein 4</i>	Accessory subunit of the mitochondrial membrane respiratory chain NADH dehydrogenase.	Complex I
BGIBMGA014059	<i>NADH dehydrogenase [ubiquinone] 1 alpha subcomplex subunit 10</i>	Accessory subunit of the mitochondrial membrane respiratory chain NADH dehydrogenase.	Complex I
BGIBMGA012356	<i>Putative secreted salivary protein</i>	NADH dehydrogenase activity.	Complex I
BGIBMGA002455	<i>NADH dehydrogenase [ubiquinone] 1 beta subcomplex subunit 2</i>	Accessory subunit of the mitochondrial membrane respiratory chain NADH dehydrogenase.	Complex I
BGIBMGA009182	<i>NADH dehydrogenase [ubiquinone] 1 beta subcomplex subunit 3</i>	Accessory subunit of the mitochondrial membrane respiratory chain NADH dehydrogenase.	Complex I
BGIBMGA011593	<i>succinate dehydrogenase cytochrome b560 subunit</i>	Membrane-anchoring subunit of succinate dehydrogenase (SDH) that is involved in complex II of the mitochondrial electron transport chain and is responsible for transferring electrons from succinate to ubiquinone (coenzyme Q).	Complex II
BGIBMGA010790	<i>succinate dehydrogenase [ubiquinone] iron-sulfur subunit</i>	Iron-sulfur protein (IP) subunit of succinate dehydrogenase (SDH) that is involved in complex II of the mitochondrial electron transport chain and is responsible for transferring electrons from succinate to ubiquinone (coenzyme Q).	Complex II
BGIBMGA013451	<i>Cytochrome c oxidase subunit NDUFA4</i>	Component of the cytochrome c oxidase, the last enzyme in the mitochondrial electron transport chain which drives oxidative phosphorylation.	Complex IV
BGIBMGA013680	<i>cytochrome c oxidase polypeptide IV</i>	Component of the cytochrome c oxidase, the last enzyme in the mitochondrial electron transport chain which drives oxidative phosphorylation.	Complex IV
BGIBMGA014175	<i>cytochrome c oxidase subunit 6C</i>	Component of the cytochrome c oxidase, the last enzyme in the mitochondrial electron transport chain which drives oxidative phosphorylation.	Complex IV

Table 1 (continued)

Gene ID	Gene name	Function	Complex of oxidative respiratory chain
BGIBMGA009700	<i>cytochrome c oxidase subunit 7C</i>	oxidative phosphorylation. Component of the cytochrome c oxidase, the last enzyme in the mitochondrial electron transport chain which drives oxidative phosphorylation.	Complex IV
BGIBMGA001853	<i>ATP synthase subunit alpha</i>	Mitochondrial membrane ATP synthase (F1FO ATP synthase or Complex V) produces ATP from ADP in the presence of a proton gradient across the membrane which is generated by electron transport complexes of the respiratory chain.	Complex V
BGIBMGA012549	<i>ATP synthase subunit beta</i>	Mitochondrial membrane ATP synthase (F1FO ATP synthase or Complex V) produces ATP from ADP in the presence of a proton gradient across the membrane which is generated by electron transport complexes of the respiratory chain.	Complex V
BGIBMGA000596	<i>V-type proton ATPase subunit H-like</i>	Subunit H activates the ATPase activity of the enzyme and couples ATPase activity to proton flow.	V-type ATPase

(Bm14) and Ebola glycoprotein.

RNA-seq analysis revealed that *Bm14* knockout mutant up-regulated the pathways associated with energy metabolism and oxidative stress. In eukaryotes, glycolysis pathway as energy sources clearly feeds into oxidative phosphorylation (Cole, 2016). The nicotinamide adenine dinucleotide (NAD^+) and reduced dinucleotide NADH are crucial for electron transport and oxidation-reduction reactions in oxidative phosphorylation pathway. Additionally, NADP^+ and NADPH are generated from NAD^+ through phosphorylation action of NAD^+ kinases, which play key roles in cellular biosynthetic pathways and in protecting cells from ROS induced damage (Anderson et al., 2017; Ying, 2008). The balance between the NAD pool and NADP pools produces profound effects on cellular functions. As shown in Table 1, the mRNA levels of several oxidative phosphorylation complexes subunits were up-regulated, suggesting that the activity of respiratory chain reactions was suppressed by *Bm14*. Moreover, it was reported that BmNPV infection resulted in a significant oxidative stress (Li et al., 2012). Thus, we surmised that *Bm14* knockout induced the increase in oxidation-reduction reactions and NAD/NADPH pool will finally enhance the ability of the host cell to resist ROS damage caused by BmNPV infection.

Consistent with our RNA-seq results, MMP and ATP assays demonstrated that BmNPV infection resulted in mitochondria dysfunction, whereas *Bm14* knockout increased MMP values and ATP concentrations (Fig. 7). Meanwhile, lower intracellular ROS levels were detected in *Bm14KO^{PH}* infected cells (Fig. 8), demonstrating that *Bm14* deletion

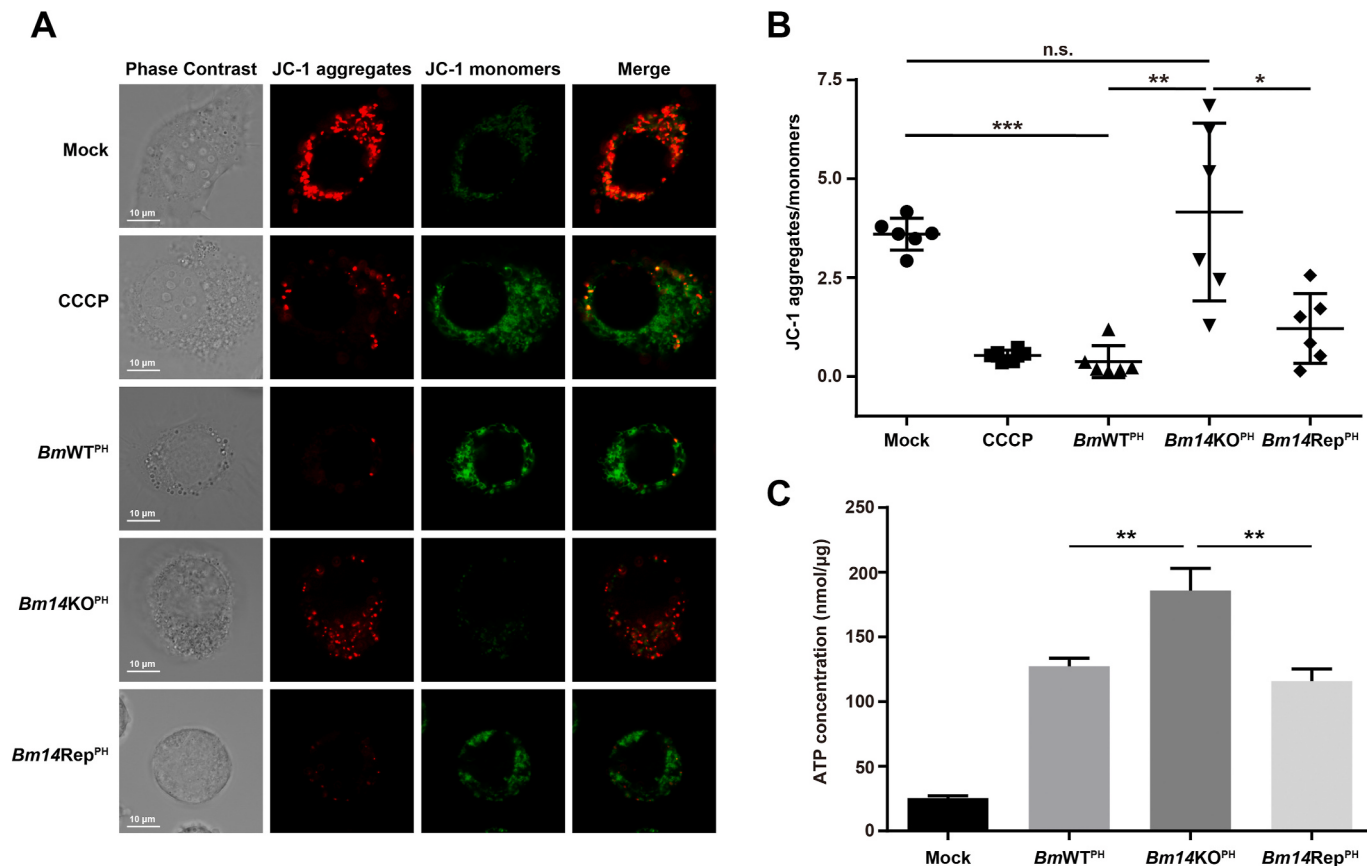


Fig. 7. Effects of *Bm14* knockout on mitochondrial membrane potential levels and ATP concentrations. (A) Confocal microscopy analysis of mitochondrial membrane potential levels indicated by JC-1 probe. Green, JC-1 monomers; red, JC-1 aggregates. **(B)** Relative ratio of JC-1 aggregates/monomers ($n = 6$; *, $p < 0.05$; **, $p < 0.01$; ***, $p < 0.001$, n.s., no significant). **(C)** ATP concentrations ($n = 3$; **, $p < 0.01$).

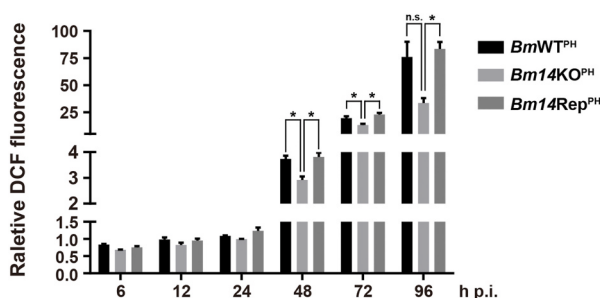


Fig. 8. *Bm14* knockout reduced intracellular ROS production. At 48 and 72 h p.i., *Bm14KO^{PH}* infected cells showed significant reductions in ROS production than *BmWT^{PH}* and *Bm14Rep^{PH}* infected cells ($n = 3$; *, $p < 0.05$; n.s., no significance).

disrupted viral infection induced mitochondria dysfunction and oxidative stress. Acceleration of oxidative stress and ROS damage were tightly associated with CPEs during viral infection (Camin et al., 2018; Douglas et al., 2016; Rajput et al., 2017; Wang et al., 2018). Therefore, we speculated that *Bm14* participated viral-induced CPEs through regulating oxidative stress responses, and the relationship between them need more explorations.

In summary, our results comprehensively demonstrate the novel functions of *Bm14* in mediating CPEs. Transcriptome analysis and biochemical assays reveal that *Bm14* might by some direct or indirect mechanism alter energy metabolism and oxidation-reduction reactions which could lead to the production of CPEs.

4. Materials and methods

4.1. Cell line, viruses, antibody and expression plasmids

The BmN cell line was cultured at 27 °C in the SF900 II SFM (Gibco) supplemented with 3% fetal bovine serum (FBS, Gibco), penicillin (100 μg/ml) and streptomycin (30 μg/ml). The T3 strain of BmNPV was termed as the wild-type (WT) virus. The recombinant viruses *BmWT^{PH}-EGFP*, *Bm14KO^{PH}-EGFP*, *Bm14Rep^{PH}-EGFP*, *BmWT^{PH}*, *Bm14KO^{PH}* and *Bm14Rep^{PH}* were previously constructed in our laboratory (Xu et al., 2019). In brief, the *Bm14* knockout virus was generated via RecE/RecT (ET) homologous recombination and the repaired virus was generated via Tn7-mediated transposition, which contained the *Bm14* driven by its native promoter (Supplementary Fig. 1 and 2). In addition, *BmWT^{PH}-EGFP* and *BmWT^{PH}* were generated as above and acted as the positive controls. Particularly, polyhedrin (PH) and EGFP were expressed independently and using the *polyhedrin* promoter and *iε1* promoter, respectively. The anti-*Bm14* polyclonal antibody was preserved by our laboratory. The expression plasmids including pIZ-EGFP, pIZ-EGFP-GP64, pIZ-mCherry and pIZ-mCherry-Bm14 were generated from the pIZ/V5-His plasmid and preserved by our laboratory (Supplementary Fig. 3).

4.2. Quantitative real-time PCR analysis (qRT-PCR)

BmN cells (1×10^6) were infected with WT, *BmWT^{PH}-EGFP*, *Bm14KO^{PH}-EGFP* or *Bm14Rep^{PH}-EGFP* at a multiplicity of infection (MOI) of 10. At the indicated time points, BmN cells were harvested and the total RNA was extracted using the TRIzol™ reagent (Invitrogen). Thereafter, 5 μg total RNA was used to synthesize the first-strand cDNAs

with the TransScript One-Step gDNA Removal and cDNA Synthesis SuperMix (TransGen). qRT-PCR was performed using Hieff® qPCR SYBR Green Master Mix (Yeasen). The primers were listed in Supplementary Table 1.

4.3. Cell detachment assay

Cell detachment assay was conducted as described previously (Simon and Linstedt, 2018) with minor modifications. In brief, cells were infected with the above-mentioned viruses at an MOI of 1 or 10 or transfected with expression plasmids at different doses. Afterwards, the media containing detached cells were collected at the indicated time points, and the adherent cells were trypsinized and harvested. The collected floating and attached cells were stained with trypan blue, and only those stained cells were counted by the cell counting board. Next, the proportion of floating cells were calculated according to the formula below: floating cells (%) = (floating cells/(floating cells + attached cells) × 100%).

4.4. Scanning electron microscopy (SEM)

SEM analysis was performed as described previously (Hacke et al., 2015b). Briefly, BmN cells were plated onto 35 mm glass-bottomed dishes, and infected with viruses or transfected with expression plasmids respectively. Thereafter, the samples were subjected to fixation, dehydration, drying at critical point, while the cells were coated with gold-palladium (5 nm). Finally, the slides were observed with the Carl Zeiss GeminiSEM 300.

4.5. Transfection with expression plasmids

For transfection assay, cells were cultured into 12-well and 96-well microplates or coverslips, respectively. Later, the Cellfectin™ II Reagent (Gibco) was adopted for transfection according to the manufacturer's instructions.

4.6. Cell viability assay

BmN cells grown in the 96-well microplates were transfected with expression plasmids or infected with various viruses. Then, the cell viability was measured using the 3-(4,5-dimethylthiazol-2-yl)-2,5-diphenyltetrazolium bromide (MTT, Invitrogen) reagent. Briefly, cells were washed thrice with PBS (pH 7.4) and incubated with 20 µl MTT reagent supplemented in 180 µl TC-100 medium for 4 h. Next, cells were washed twice with PBS (pH 7.4) and dissolved into 200 µl Formazan solvent. Later, the sample absorbances were measured with the spectrophotometer at the wavelength of 570 nm.

4.7. Immunofluorescence assay

BmN cells were plated onto 35 mm glass-bottomed dishes and transfected with Cellfectin™ II reagent. At 48 h post-transfection, cells were washed twice with PBS (pH 7.4) and fixed within the 4% paraformaldehyde for 20 min. Afterwards, cells were permeabilized in 0.1% TritonX-100, blocked with 0.5% BSA/PBS, and incubated with rabbit polyclonal anti-Bm14 antibody (dilution 1:500) overnight at 4 °C. Next, the samples were incubated with Alexa 488-conjugated donkey anti-rabbit antibody (dilution 1:500, Invitrogen). Then, cells were sealed in 4',6'-diamidino-2-phenylindole (DAPI, Beyotime) and examined using a ZEISS LSM 780 confocal laser scanning microscopy.

4.8. RNA-seq

RNA-seq libraries were prepared as described previously (Liu et al., 2017) with some modifications. Briefly, the cells were infected with recombinant viruses *BmWT*^{PH-EGFP} and *Bm14KO*^{PH-EGFP} at an MOI of 10.

Total RNA was extracted using the TRIzol™ reagent (Invitrogen) according to the manufacturer's instructions. Approximately 3 µg of RNA per sample was used as the input material for library preparation. The libraries were constructed using the NEBNext Ultra™ RNA Library Prep Kit for Illumina (NEB), and the index codes were added to attribute the sequences to each sample. Then the obtained libraries were sequenced on the HiSeq X ten illumina platform with a paired-end read of 150 bp.

The raw RNA-seq data quality was evaluated by the FastQC program, and the sequencing adaptors were trimmed by Trimmomatic (Bolger et al., 2014). Later, the filtered reads were aligned to the reference *Bombyx mori* genome using STAR (Dobin et al., 2013), and only the uniquely mapped reads were preserved, while the BmNPV reads were removed. The read counts and RPKM were calculated by HTSeq (Anders et al., 2015).

To characterize the differentially expressed genes (DEGs), the transcripts of *Bm14KO*^{PH-EGFP} infected cells were compared with those of *BmWT*^{PH-EGFP} (indicated as control). Those genes that had two-fold changes between the control transcripts and p.adjust was less than 0.05 were identified as DEGs. For functional analysis, KEGG pathway (<http://www.kegg.jp/>) was performed to identify the biological pathways altered in response to *Bm14*-null mutant infection.

4.9. Detection of mitochondrial membrane potential

The mitochondrial membrane potential was measured using the JC-1 kit (Beyotime) according to the manufacturer's instruction. Briefly, the BmN cells were treated with 10 µM CCCP or infected with recombinant viruses. At 48 h p.i., the cells were stained with JC-1 probe, and then examined using a ZEISS LSM 780 confocal laser scanning microscopy.

4.10. Adenosine triphosphate (ATP) assay

ATP concentration was measured using ATP Assay Kit (Beyotime) according to the manufacturer's instruction. Briefly, the BmN cells were infected with recombinant viruses. At 48 h p.i., the cells were lysed and then centrifuged to collect supernatants. Relative intensity of the luminescence was measured by SYNERGY HTX microplate reader. Protein concentrations were measured using a BCA kit (Takara).

4.11. Intracellular ROS level measurement

Intracellular ROS levels were determined by staining cells with dichlorofluorescin diacetate (DCFH-DA, Yeasen). Briefly, the BmN cells were infected with recombinant viruses. At indicated times, the cells were washed with PBS and incubated with 10 µM DCFH-DA at 27 °C for 30 min. Cells were then washed twice with PBS and analyzed by flow cytometry (BD FACSVerser™).

Declaration of competing interest

The authors declare that no conflict of interest exists in the submission of this manuscript, and this manuscript is approved by all authors for publication. The founders had no role in study design, data collection and analysis, decision to publish, or preparation of the manuscript.

Acknowledgement

We are grateful to Bio-ultrastructure Lab of Analysis Center at Zhejiang University for technical assistance.

This study was supported by the National Natural Science Foundation of China (project 31772675 and 31972619) and the Natural Science Foundation of Zhejiang Province (Z20C170008). We declare that there is no conflict of interest in our work.

Appendix A. Supplementary data

Supplementary data to this article can be found online at <https://doi.org/10.1016/j.virol.2020.10.001>.

Author contributions

X.F.W conceived and designed the experiments, revised the manuscript. X.S.K designed this study, performed the experiments, processed the data and wrote the manuscript. W.F.X provided the materials and reviewed the manuscript. N.C, Y.L and Y.W.S performed the manuscript.

References

- Agol, V.I., 2012. Cytopathic effects: virus-modulated manifestations of innate immunity? *Trends Microbiol.* 20, 570–576.
- Anders, S., Pyl, P.T., Huber, W., 2015. HTSeq—a Python framework to work with high-throughput sequencing data. *Bioinformatics* (Oxford, England) 31, 166–169.
- Anderson, K.A., Madsen, A.S., Olsen, C.A., Hirshey, M.D., 2017. Metabolic control by sirtuins and other enzymes that sense NAD(+), NADH, or their ratio. *Biochim. Biophys. Acta Bioenerg.* 1858, 991–998.
- Blissard, G.W., Theilmann, D.A., 2018. Baculovirus entry and egress from insect cells. *Annu Rev Virol* 5, 113–139.
- Blissard, G.W., Wenz, J.R., 1992. Baculovirus gp64 envelope glycoprotein is sufficient to mediate pH-dependent membrane fusion. *J. Virol.* 66, 6829–6835.
- Bolger, A.M., Lohse, M., Usadel, B., 2014. Trimmomatic: a flexible trimmer for Illumina sequence data. *Bioinformatics* (Oxford, England) 30, 2114–2120.
- Camini, F.C., da Silva, T.F., da Silva Caetano, C.C., Almeida, L.T., Ferraz, A.C., Alves Vitoreti, V.M., de Mello Silva, B., de Queiroz Silva, S., de Magalhães, J.C., de Brito Magalhães, C.L., 2018. Antiviral activity of silymarin against Mayaro virus and protective effect in virus-induced oxidative stress. *Antivir. Res.* 158, 8–12.
- Cerio, R.J., Vandergaast, R., Friesen, P.D., 2010. Host insect inhibitor-of-apoptosis SIAP functionally replaces baculovirus IAP but is differentially regulated by its N-terminal leader. *J. Virol.* 84, 11448–11460.
- Cole, L.A., 2016. Chapter 10 - adenosine triphosphate energetics. In: Cole, L.A. (Ed.), *Biology of Life*. Academic Press, pp. 65–77.
- Cossarizza, A., Baccarancontri, M., Kalashnikova, G., Franceschi, C., 1993. A new method for the cytofluorometric analysis of mitochondrial membrane potential using the J-aggregate forming lipophilic cation 5,5',6,6'-Tetrachloro-1,1',3,3'-tetraethylbenzimidazolcarbocyanine iodide (JC-1). *Biochem. Biophys. Res. Commun.* 197, 40–45.
- Curtin, F., Bernard, C., Levet, S., Perron, H., Porchet, H., Médina, J., Malpass, S., Lloyd, D., Simpson, R., 2018. A new therapeutic approach for type 1 diabetes: rationale for GnbaCl, an anti-HERV-W-Env monoclonal antibody. *Diabetes Obes. Metabol.* 20, 2075–2084.
- Dobin, A., Davis, C.A., Schlesinger, F., Drenkow, J., Zaleski, C., Jha, S., Batut, P., Chaisson, M., Gingeras, T.R., 2013. STAR: ultrafast universal RNA-seq aligner. *Bioinformatics* (Oxford, England) 29, 15–21.
- Dong, S., Wang, M., Qiu, Z., Deng, F., Vlak, J.M., Hu, Z., Wang, H., 2010. *Autographa californica* multicapsid nucleopolyhedrovirus efficiently infects SF9 cells and transduces mammalian cells via direct fusion with the plasma membrane at low pH. *J. Virol.* 84, 5351–5359.
- Dong, X.L., Liu, T.H., Wang, W., Pan, C.X., Wu, Y.F., Du, G.Y., Chen, P., Lu, C., Pan, M.H., 2015. BmREEPa is a novel gene that facilitates BmNPV entry into silkworm cells. *PloS One* 10, e0144575.
- Douglas, D.N., Pu, C.H., Lewis, J.T., Bhat, R., Anwar-Mohamed, A., Logan, M., Lund, G., Addison, W.R., Lehner, R., Kneteman, N.M., 2016. Oxidative stress attenuates lipid synthesis and increases mitochondrial fatty acid oxidation in hepatoma cells infected with hepatitis C virus. *J. Biol. Chem.* 291, 1974–1990.
- Francica, J.R., Matukonis, M.K., Bates, P., 2009. Requirements for cell rounding and surface protein down-regulation by Ebola virus glycoprotein. *Virology* 383, 237–247.
- Hacke, M., Björkholm, P., Hellwig, A., Himmels, P., Ruiz de Almodovar, C., Brügger, B., Wieland, F., Ernst, A.M., 2015a. Inhibition of Ebola virus glycoprotein-mediated cytotoxicity by targeting its transmembrane domain and cholesterol. *Nat. Commun.* 6, 7688.
- Hacke, M., Björkholm, P., Hellwig, A., Himmels, P., Ruiz de Almodóvar, C., Brügger, B., Wieland, F., Ernst, A.M., 2015b. Inhibition of Ebola virus glycoprotein-mediated cytotoxicity by targeting its transmembrane domain and cholesterol. *Nat. Commun.* 6, 7688.
- Hefferon, K.L., Oomens, A.G., Monsma, S.A., Finnerty, C.M., Blissard, G.W., 1999. Host cell receptor binding by baculovirus GP64 and kinetics of virion entry. *Virology* 258, 455–468.
- Huang, J., Li, J., Cheng, C., Tang, X., Shen, X., Hao, B., 2019. An amino acid duplication/insertion in the Bm126 gene of *Bombyx mori* nucleopolyhedrovirus alters viral gene expression as shown by differential gene expression analysis. *Arch. Virol.* 164, 831–838.
- Huang, N., Wu, W., Yang, K., Passarelli, A.L., Rohrmann, G.F., Clem, R.J., 2011. Baculovirus infection induces a DNA damage response that is required for efficient viral replication. *J. Virol.* 85, 12547–12556.
- Kamita, S.G., Maeda, S., 1993. Inhibition of *Bombyx mori* nuclear polyhedrosis virus (NPV) replication by the putative DNA helicase gene of *Autographa californica* NPV. *J. Virol.* 67, 6239–6245.
- Katou, Y., Yamada, H., Ikeda, M., Kobayashi, M., 2010. A single amino acid substitution modulates low-pH-triggered membrane fusion of GP64 protein in *Autographa californica* and *Bombyx mori* nucleopolyhedroviruses. *Virology* 404, 204–214.
- Levin, D.B., Huang, J., 1999. Spodoptera littoralis type B nucleopolyhedrovirus infection of a grasshopper cell line. *J. Invertebr. Pathol.* 74, 184–192.
- Li, B., Xie, Y., Cheng, Z., Cheng, J., Hu, R., Cui, Y., Gong, X., Shen, W., Hong, F., 2012. Effects of added CeCl₃ on resistance of fifth-instar larvae of silkworm to *Bombyx mori* nucleopolyhedrovirus infection. *Biol. Trace Elem. Res.* 146, 318–324.
- Liu, Y., Su, H., Li, R., Li, X., Xu, Y., Dai, X., Zhou, Y., Wang, H., 2017. Comparative transcriptome analysis of *Glyptodes pyralis* Walker (Lepidoptera: Pyralidae) reveals novel insights into heat stress tolerance in insects. *BMC Genom.* 18, 974.
- Lung, O., Westenberg, M., Vlak, J.M., Zuidema, D., Blissard, G.W., 2002. Pseudotyping *Autographa californica* multicapsid nucleopolyhedrovirus (AcMNPV): F proteins from group II NPVs are functionally analogous to AcMNPV GP64. *J. Virol.* 76, 5729–5736.
- Lung, O.Y., Cruz-Alvarez, M., Blissard, G.W., 2003. Ac23, an envelope fusion protein homolog in the baculovirus *Autographa californica* multicapsid nucleopolyhedrovirus, is a viral pathogenicity factor. *J. Virol.* 77, 328–339.
- McGettigan, J.P., Foley, H.D., Belyakov, I.M., Berzofsky, J.A., Pomerantz, R.J., Schnell, M.J., 2001. Rabies virus-based vectors expressing human immunodeficiency virus type 1 (HIV-1) envelope protein induce a strong, cross-reactive cytotoxic T-lymphocyte response against envelope proteins from different HIV-1 isolates. *J. Virol.* 75, 4430–4434.
- Melkonian, E.A., Zafar Gondal, A., Schury, M.P., 2020. *Physiology, Gluconeogenesis*. StatPearls Publishing.
- Mi, S., Lee, X., Li, X., Veldman, G.M., Finnerty, H., Racine, L., LaVallie, E., Tang, X.Y., Edouard, P., Howes, S., Keith Jr., J.C., McCoy, J.M., 2000. Syncytin is a captive retroviral envelope protein involved in human placental morphogenesis. *Nature* 403, 785–789.
- Mitchell, J.K., Friesen, P.D., 2012. Baculoviruses modulate a proapoptotic DNA damage response to promote virus multiplication. *J. Virol.* 86, 13542–13553.
- Nagamine, T., Kawasaki, Y., Abe, A., Matsumoto, S., 2008. Nuclear marginalization of host cell chromatin associated with expansion of two discrete virus-induced subnuclear compartments during baculovirus infection. *J. Virol.* 82, 6409–6418.
- Netherton, C., Moffat, K., Brooks, E., Wileman, T., 2007. A guide to viral inclusions, membrane rearrangements, factories, and viroplasm produced during virus replication. *Adv. Virus Res.* 70, 101–182.
- Pearson, M.N., Russell, R.L., Rohrmann, G.F., 2001. Characterization of a baculovirus-encoded protein that is associated with infected-cell membranes and budded virions. *Virology* 291, 22–31.
- Pereira, H.G., 1961. The cytopathic effect of animal viruses. *Adv. Virus Res.* 8, 245–285.
- Rajput, M.K.S., Abdelsalam, K., Darweesh, M.F., Braun, L.J., Kerkvliet, J., Hoppe, A.D., Chase, C.C.L., 2017. Both cytopathic and non-cytopathic bovine viral diarrhea virus (BVDV) induced autophagy at a similar rate. *Vet. Immunol. Immunopathol.* 193–194, 1–9.
- Rohrmann, G.F., 2019. *Baculovirus Molecular Biology*. National Center for Biotechnology Information (US), Bethesda (MD).
- Rohrmann, G.F., Karplus, P.A., 2001. Relatedness of baculovirus and gypsy retrotransposon envelope proteins. *BMC Evol. Biol.* 1, 1.
- Santos, S.A., Silva, J.L., Balani, V.A., Seixas, F.A., Fernandez, M.A., 2010. Conserved baculoviral ORFs 10 and 14 from *Bombyx mori* multiple nucleopolyhedrovirus. *Genet. Mol. Res.* : GMR 9, 457–470.
- Schultz, K.L., Friesen, P.D., 2009. Baculovirus DNA replication-specific expression factors trigger apoptosis and shutdown of host protein synthesis during infection. *J. Virol.* 83, 11123–11132.
- Simon, E.J., Linstedt, A.D., 2018. Site-specific glycosylation of Ebola virus glycoprotein by human polypeptide GalNAc-transferase 1 induces cell adhesion defects. *J. Biol. Chem.* 293, 19866–19873.
- Stamatatos, L., Cheng-Mayer, C., 1993. Evidence that the structural conformation of envelope gp120 affects human immunodeficiency virus type 1 infectivity, host range, and syncytium-forming ability. *J. Virol.* 67, 5635–5639.
- van Oers, M.M., Vlak, J.M., 2007. Baculovirus genomics. *Curr. Drug Targets* 8, 1051–1068.
- Wang, Q.W., Su, Y., Sheng, J.T., Gu, L.M., Zhao, Y., Chen, X.X., Chen, C., Li, W.Z., Li, K.S., Dai, J.P., 2018. Anti-influenza A virus activity of rhein through regulating oxidative stress, TLR4, Akt, MAPK, and NF-κB signal pathways. *PloS One* 13, e0191793.
- Wang, W., Jobbagy, Z., Bird, T.H., Eiden, M.V., Anderson, W.B., 2005. Cell signaling through the protein kinases cAMP-dependent protein kinase, protein kinase Cepsilon, and RAF-1 regulates amphotropic murine leukemia virus envelope protein-induced syncytium formation. *J. Biol. Chem.* 280, 16772–16783.
- Westenberg, M., Wang, H., Wf, I.J., Goldbach, R.W., Vlak, J.M., Zuidema, D., 2002. Furin is involved in baculovirus envelope fusion protein activation. *J. Virol.* 76, 178–184.
- Whittome-Waygood, B.H., Fraser, J.C., Lucarotti, C.J., Otvos, I.S., Conder, N., Levin, D.B., 2009. In vitro culture of *Lambdina fiscellaria* lugubrosa nucleopolyhedrovirus in heterologous cell lines. In vitro cellular & developmental biology. Animal 45, 300–309.
- Xu, W., Fan, Y., Wang, H., Feng, M., Wu, X., 2019. *Bombyx mori* nucleopolyhedrovirus F-like protein Bm14 affects the morphogenesis and production of occlusion bodies and the embedding of ODVs. *Virology* 526, 61–71.
- Xu, W., Kong, X., Liu, H., Wang, H., Wu, X., 2020. *Bombyx mori* nucleopolyhedrovirus F-like protein Bm14 is a type I integral membrane protein that facilitates ODV attachment to the midgut epithelial cells. *J. Gen. Virol.* 101, 309–321.

- Xu, W., Wang, H., Liu, H., Wu, X., 2020. *Bombyx mori* nucleopolyhedrovirus F-like protein Bm14 is a cofactor for GP64-Mediated efficient infection via forming a complex on the envelope of budded virus. *Virology* 539, 61–68.
- Yang, Z.Y., Duckers, H.J., Sullivan, N.J., Sanchez, A., Nabel, E.G., Nabel, G.J., 2000. Identification of the Ebola virus glycoprotein as the main viral determinant of vascular cell cytotoxicity and injury. *Nat. Med.* 6, 886–889.
- Ying, W., 2008. NAD+/NADH and NADP+/NADPH in cellular functions and cell death: regulation and biological consequences. *Antioxidants Redox Signal.* 10, 179–206.
- Zhang, P., Yang, K., Dai, X., Pang, Y., Su, D., 2002. Infection of wild-type *Autographa californica* multicapsid nucleopolyhedrovirus induces in vivo apoptosis of *Spodoptera litura* larvae. *J. Gen. Virol.* 83, 3003–3011.
- Zhou, J., Blissard, G.W., 2008. Identification of a GP64 subdomain involved in receptor binding by budded virions of the baculovirus *Autographica californica* multicapsid nucleopolyhedrovirus. *J. Virol.* 82, 4449–4460.